

# Direct derivation of anisotropic atomic displacement parameters from molecular dynamics simulations demonstrated in thermoelectric materials

**Yoyo Hinuma**

Department of Energy and Environment, National Institute of Advanced Industrial Science and Technology (AIST), 1-8-31, Midorigaoka, Ikeda, Osaka 563-8577, Japan

\*y.hinuma@aist.go.jp

## **ABSTRACT:**

Atomic displacement parameters (ADPs) are crystallographic information that describe the statistical distribution of atoms around an atom site. Direct derivation of anisotropic ADPs by atom from molecular dynamics (MD) simulations, where the (co)valences of atom positions are taken over recordings at different time steps in a single MD simulation, was demonstrated on three thermoelectric materials,  $\text{Ag}_8\text{SnSe}_6$ ,  $\text{Na}_2\text{In}_2\text{Sn}_4$ , and  $\text{BaCu}_{1.14}\text{In}_{0.86}\text{P}_2$ . Unlike the very frequently used lattice dynamics approach, the MD approach can obtain ADPs in disordered crystals and at finite temperature, but not under conditions where atoms migrate in the crystal. ADPs from MD simulations would act as a tool complementing experimental efforts to understand the crystal structure including the distribution of atoms around atom sites.

## **1. Introduction**

Atomic displacement parameters (ADPs) are often provided as part of crystal crystallographic structural data and may represent atomic motion, possible static displacive disorder, and thermal vibration. (Trueblood *et al.*, 1996) ADPs are generally anisotropic. Calculation of ADPs are important especially to model those of light elements such as H, where obtaining ADPs from X-ray diffraction is difficult, and to provide clues for obtaining a better picture of the actual crystal structure through refinement.

Theoretical derivations of ADPs are typically performed indirectly through lattice dynamics analysis, where the dynamical matrix is obtained and the vibrational, or phonon, frequency of each mode is calculated. Examples of formalisms are found in Erba *et al.* (Erba *et al.*, 2013), Madsen *et al.* (Madsen *et al.*, 2013), and Lane *et al.* (Lane *et al.*, 2012)

The lattice dynamics approach is difficult to apply in systems where disorder of elements

on a (sub)lattice plays a critical role. Models with large supercells and/or a very short range order on the (sub)lattice is required and the symmetry is different from the experimental model. The effect of ordering may significantly affect the final results in a small supercell with short range ordering.

Split-site systems are also problematic with lattice dynamics. One example of a split site is a double-well potential with minima at two very close positions. The average position of an atom at this site will be the middle of the two positions at elevated temperatures, while the atom will be at one of the minima at the 0 K limit. Placing the atom at the elevated temperature position leads to an imaginary mode at the  $\Gamma$  point.

On the other hand, direct derivation of anisotropic ADPs, assuming a normal (or Gaussian) distribution, from molecular dynamics (MD) simulations is possible even for disordered systems and split site systems. The averages of displacement vector components from the mean atom position, such as  $\langle \Delta \zeta_i^C \Delta \zeta_j^C \rangle$ , are simply the covariances of atom positions, for instance  $\text{Cov}(\Delta \zeta_{i+\zeta_i}^C, \Delta \zeta_{j+\zeta_j}^C)$ . Here,  $\zeta_i^C$  and  $\Delta \zeta_i^C$  are the  $i$ -component of the mean atom position vector and the displacement vector, respectively, in Cartesian coordinates for a given atom. A large number of displacement values for a given crystal can be obtained from MD simulations, and derivation of ADPs from these values is very straightforward. This approach was used in the literature to obtain the anisotropic ADPs of  $\text{ND}_3$  (Reilly *et al.*, 2007) and benzophenone (Reilly *et al.*, 2013).

The ADP of an individual atom and that of an atom site must be clearly distinguished. The (co)variance of positions for a single atom is obtained in the former, while the (co)variance in the latter is taken over positions of multiple atoms that are each affine transformed such that the images of atoms are at almost the same position. Experimentally, the latter is much easier to obtain. The intrinsic displacements of atoms from the center of the atom site, which is unavoidable in a disordered crystal with partial occupancies in some sites though the extent depends on the system, and the displacements caused by thermal fluctuation are lumped together in the latter description of the ADP. In contrast, the former ADP is straightforwardly obtained from calculations, while the latter can be derived through further processing.

The ADPs of an individual atom is exactly proportional to temperature for an isolated atom in a harmonic potential, according to quantum mechanics (Hinuma, 2025). Significant deviations from proportionality are caused by an anharmonic potential,

although what causes the anharmonicity cannot be identified from this information only and the converse does not necessarily hold.

The direct method can, in principle, derive ADPs for any system. One notable exception is when atoms migrate during the simulations and are not trapped around an equilibrium point. The drawback of the direct method is that each MD simulation gives different results and obtaining very reliable values require a long simulation time and/or a large supercell, which could be computationally expensive using first-principles calculations.

This paper demonstrates use of universal neural network potential (NNP) MD simulations to obtain the ADP in three thermoelectric materials, namely argyrodite structure  $\text{Ag}_8\text{SnSe}_6$  (Takahashi *et al.*, 2024),  $\text{Na}_2\text{In}_2\text{Sn}_4$  (Yamada *et al.*, 2023) with a helical tunnel framework structure, and ThCr<sub>2</sub>Si<sub>2</sub>-type phosphide  $\text{BaCu}_{1.14}\text{In}_{0.86}\text{P}_2$  (Sarkar *et al.*, 2024). The crystal structures are visualized in Fig. 1. The calculated ADPs are compared with experimentally reported values. The ADPs are especially interesting in thermoelectric materials because rattling atoms with large ADPs, which may be very anisotropic, could be effective in reducing the thermal conductivity and improving the thermoelectric performance.

## 2. Formalism

Various symbols are used in the literature to describe ADPs, including  $\mathbf{U}$ ,  $\mathbf{U}^C$ ,  $\mathbf{B}$ , and  $\boldsymbol{\beta}$ , and these have not always been used consistently. Table 1 summarizes the recommendations from a subcommittee on ADP nomenclature from the International Union of Crystallography (from section 1.3 of Trueblood *et al.* (Trueblood *et al.*, 1996)). Here,  $\mathbf{r}$  is the mean atom position vector and  $\mathbf{u}$  is the displacement vector from  $\mathbf{r}$ . The basis vector lengths of the reciprocal axes are denoted as  $a^*$ ,  $b^*$ , and  $c^*$  or  $a^1$ ,  $a^2$ , and  $a^3$ .

The CIF format uses  $\mathbf{U}$ , while the PDB convention adopts  $\mathbf{U}^C$ . (Grosse-Kunstleve & Adams, 2002) The  $\mathbf{U}$  and  $\mathbf{U}^C$  are identical only when the basis vectors are orthogonal to each other.

The  $\mathbf{U}$ ,  $\boldsymbol{\beta}$ , and  $\mathbf{B}$  are related by (equation 38 in ref. (Trueblood *et al.*, 1996))

$$U^{jl} = \beta^{jl} / (2\pi^2 a^j a^l) = B^{jl} / 8\pi^2. \quad (1)$$

Using a scaling matrix

$$\mathbf{S} = \begin{pmatrix} a^* & 0 & 0 \\ 0 & b^* & 0 \\ 0 & 0 & c^* \end{pmatrix}, (2)$$

$$\beta = 2\pi^2 \mathbf{S} \mathbf{U} \mathbf{S}. (3)$$

The Debye-Waller factor for a diffraction vector

$$\mathbf{h} = \sum_{i=1}^3 h_i \mathbf{a}^i = \sum_{i=1}^3 h_i^C \mathbf{e}_i, (4)$$

a row vector in reciprocal space, is

$$\begin{aligned} T(\mathbf{h}) &= \exp \left( - \sum_{j=1}^3 \sum_{l=1}^3 h_j \beta^{jl} h_l \right) \\ &= \exp \left( -2\pi^2 \sum_{j=1}^3 \sum_{l=1}^3 h_j a^j U^{jl} a^l h_l \right) (5) \\ &= \exp \left( -2\pi^2 \sum_{j=1}^3 \sum_{l=1}^3 h_j^C U_{jl}^C h_l^C \right) \end{aligned}$$

(equations 21, 24, 34, and 36 in ref. (Trueblood *et al.*, 1996)). Here,  $(\mathbf{e}_1, \mathbf{e}_2, \mathbf{e}_3)$  is an orthonormal basis.

One transformation matrix between the bases  $(\mathbf{a}, \mathbf{b}, \mathbf{c})$  and  $(\mathbf{e}_1, \mathbf{e}_2, \mathbf{e}_3)$  is (equation 50 in ref. (Trueblood *et al.*, 1996))

$$\mathbf{A} = \begin{pmatrix} a & b \cos \gamma & c \cos \beta \\ 0 & b \sin \beta & -c \sin \beta \cos \alpha^* \\ 0 & 0 & 1/c^* \end{pmatrix}. (6)$$

Coordinates of vector  $\mathbf{r}$  in bases  $(\mathbf{a}, \mathbf{b}, \mathbf{c})$ ,  $(a^* \mathbf{a}, b^* \mathbf{b}, c^* \mathbf{c})$ , and  $(\mathbf{e}_1, \mathbf{e}_2, \mathbf{e}_3)$ , which are denoted as  $(x, y, z)$ ,  $(\zeta, \eta, \zeta)$ , and  $(\zeta^C, \eta^C, \zeta^C)$ , respectively, transform as

$$(\zeta^C, \eta^C, \zeta^C)^T = \mathbf{A} (x, y, z)^T (7)$$

(based on equation 41 in ref. (Trueblood *et al.*, 1996)) and

$$(\zeta^C, \eta^C, \zeta^C)^T = \mathbf{A} \mathbf{S} (\zeta, \eta, \zeta)^T (8)$$

(based on equations 46-48 in ref. (Trueblood *et al.*, 1996)). Matrix

$$\mathbf{D} = \mathbf{A} \mathbf{S} (9)$$

is used in ref. (Trueblood *et al.*, 1996).

The transformation between  $\mathbf{U}$  with the basis  $(a^* \mathbf{a}, b^* \mathbf{b}, c^* \mathbf{c})$  and  $\mathbf{U}^C$  with the orthonormal

basis ( $\mathbf{e}_1, \mathbf{e}_2, \mathbf{e}_3$ ) is

$$\mathbf{U}^C = \mathbf{A}\mathbf{S}\mathbf{U}\mathbf{S}\mathbf{A}^T = \mathbf{D}\mathbf{U}\mathbf{D}^T \quad (10)$$

(based on equation 49 in ref. (Trueblood *et al.*, 1996)).

The ADPs of an atom are often visualized as an ellipsoid. The principal semi-axes of the ellipsoid are simply the three eigenvalues of  $\mathbf{U}^C$ , and the directions of the semi-axes are those of the eigenvectors. The matrix of three eigenvectors  $\mathbf{P}$  and the diagonal matrix with three corresponding eigenvalues  $\mathbf{Q}$  are obtained as

$$\mathbf{P}^{-1}\mathbf{U}^C\mathbf{P} = \mathbf{Q} \quad (11)$$

The eigenvectors in the bases ( $\mathbf{a}, \mathbf{b}, \mathbf{c}$ ) and ( $a^*\mathbf{a}, b^*\mathbf{b}, c^*\mathbf{c}$ ) are derived with equations (7) and (8), respectively. Alternatively, principal component analysis may be used to obtain the eigenvalues and eigenvectors of  $\mathbf{U}^C$ .

The conversion of  $\mathbf{U}$  between two atoms with the same Wyckoff position,  $p$  and  $q$ , are given below. Let the mean positions of the two atoms  $p$  and  $q$ ,  $\mathbf{r} = (x, y, z)^T$  and

$\mathbf{r}' = (x', y', z')^T$ , be related as

$$\mathbf{r}' = \mathbf{R}\mathbf{r} + \mathbf{t} \quad (12)$$

where  $\mathbf{R}$  is a rotation matrix and  $\mathbf{t}$  is a translation vector. The relation between displacement vectors  $\mathbf{u} = (\Delta x, \Delta y, \Delta z)^T$  and  $\mathbf{u}' = (\Delta x', \Delta y', \Delta z')^T$  is

$$\mathbf{u}' = \mathbf{R}\mathbf{u} \quad (13)$$

The goal here is to change the basis vectors defining  $\mathbf{U}'$  such that the transformed quantity  $\mathbf{U}''$  is directly comparable to  $\mathbf{U}$ , which is accomplished by

$$\mathbf{U}'' = (\mathbf{R}^{-1})\mathbf{U}'(\mathbf{R}^{-1})^T \quad (14)$$

This transformation is useful to increase the number of atoms with  $\mathbf{U}$  values that can be easily averaged, thereby improving the reliability of results. The average  $\mathbf{U}$  and  $\mathbf{U}^C$  of atoms that are directly comparable is simply the mean of  $\mathbf{U}$  and  $\mathbf{U}^C$  of the atoms, respectively.

### 3. Methodology

#### 3.1 MD procedure

MD simulations were conducted using the commercially available Matlantis package from Preferred Networks with their universal PrePreferred Potential (PPF) (Takamoto *et al.*,

2022) version 7.0.0, a NNP trained on the Perdew-Burke-Ernzerhof (PBE) generalized gradient approximation (GGA) to density functional theory (DFT) (Perdew *et al.*, 1996). Using the NNP instead of first-principles calculations results in accumulation of atom positions with a pace that is orders of magnitude faster. The PFP is already fully trained by the developers based on calculations using the VASP code (Kresse & Furthmüller, 1996; Kresse & Joubert, 1999) and is available as a “take it or leave it” potential; the user cannot modify it. The canonical, or constant number of atoms, volume, and temperature (NVT), ensemble was used with a Nosé–Hoover thermostat (Nosé, 1984; Hoover, 1985). The objective of this paper is to demonstrate direct derivation of ADPs from MD simulations using a reasonable energy and force calculator, and fine-tuning the NNP for individual compounds is outside the scope.

Structural and calculation details of the considered crystals are described below.

### 3.2. $\text{Ag}_8\text{SnSe}_6$ simulations

The unit cell of  $\text{Ag}_8\text{SnSe}_6$  contains 30 atoms and its space group type is  $Pmn2_1$  (number 31). The experimental lattice parameters at 300 K are  $a = 7.91440 \text{ \AA}$ ,  $b = 7.82954 \text{ \AA}$ , and  $c = 11.05912 \text{ \AA}$ , which were used for MD simulations. The Ag atoms rattle and are of interest in this study. There are five symmetrically different Ag sites. The Wyckoff positions of sites Ag1, Ag2, and Ag3 are  $4b$ , and those of Ag4 and Ag5 are  $2a$  (Takahashi *et al.*, 2024).

$2 \times 2 \times 2$  and  $3 \times 3 \times 3$  supercells were built for MD simulations of  $\text{Ag}_8\text{SnSe}_6$ . The time step was 2 fs, and the number of steps was 140,000 and 45,000 steps, respectively (280 and 90 ps, respectively). Positions were recorded every 100 steps, but the positions for the first 5,000 steps (10 ps, 50 position recordings, hereafter equilibration steps) were discarded to account for initial shifting of atoms to attain equilibration. The number of Na position data is the same in the two calculations ( $16 \times 2 \times 2 \times 2$  Ag atoms  $\times$  1350 position recordings and  $16 \times 3 \times 3 \times 3$  Ag atoms  $\times$  400 position recordings). The temperature  $T$  was varied between 50 to 300 K in 50 K intervals.

The  $\mathbf{U}$  for each Ag atom in a MD simulation was obtained by taking the (co)variances of atom positions from position recordings. The symmetrically equivalent coordinate triplets for  $4a$  sites are  $(x,y,z)$ ,  $(-x+1/2,-y,z+1/2)$ ,  $(x+1/2,-y,-z+1/2)$ , and  $(-x,y,z)$ . The  $\mathbf{U}$  for the second, third, and fourth types of atoms can be transformed to  $\mathbf{U}$  for the first type, which is reported in this paper, using a matrix  $\mathbf{R}$  (equation 12) that is a diagonal matrix with

diagonal components  $(-1,-1,1)$ ,  $(1,-1,1)$ , and  $(-1,1,1)$ , respectively. For  $2a$  sites with equivalent coordinate triplets  $(0,y,z)$  and  $(0,-y,z+1/2)$ , the diagonal matrix  $\mathbf{R}$  of the latter has diagonal components  $(1,-1,1)$ . The final  $\mathbf{U}$  value of each Wyckoff position of Ag was derived by averaging the  $\mathbf{U}$ , for each atom, over all atoms in all simulations.

### 3.3. $\text{Na}_2\text{In}_2\text{Sn}_4$ simulations

The unit cell of  $\text{Na}_2\text{In}_2\text{Sn}_4$  contains 16 atoms and its space group type is  $P2_12_12_1$  (number 19). The experimental lattice parameters at 300 K are  $a = 6.3091 \text{ \AA}$ ,  $b = 6.5632 \text{ \AA}$ , and  $c = 11.3917 \text{ \AA}$ , which were used for MD simulations. There are four  $4a$  sites, where one is fully occupied by Na and the other three are shared by In and Sn with a 1:2 ratio. Na has high anisotropy and rattle in this compound. (Yamada *et al.*, 2023)

For  $\text{Na}_2\text{In}_2\text{Sn}_4$ ,  $4 \times 4 \times 2$  supercells were built containing 128 Na sites and 384 In/Sn sites. 10 supercells, where 128 In and 256 Sn atoms were randomly assigned to the 384 In/Sn sites, were built as initial structures. The time step was 2 fs, positions were recorded every 100 steps, and 55,000 steps (110 ps, 500 position recordings) were considered. The first 5,000 steps (10 ps, 50 position recordings) were discarded as equilibration steps. The temperature  $T$  was varied between 50 to 300 K in 50 K intervals.

The final  $\mathbf{U}$  was obtained similarly as in  $\text{Ag}_8\text{SnSe}_6$ . The symmetrically equivalent coordinate triplets for  $4a$  sites are  $(x,y,z)$ ,  $(-x+1/2,-y,z+1/2)$ ,  $(-x,y+1/2,-z+1/2)$ , and  $(x+1/2,-y+1/2,-z)$ . The  $\mathbf{U}$  for the second, third, and fourth types of atoms can be transformed to  $\mathbf{U}$  for the first type, which is reported in this paper, using a matrix  $\mathbf{R}$  (equation 12) that is a diagonal matrix with diagonal components  $(-1,-1,1)$ ,  $(-1,1,-1)$ , and  $(1,-1,-1)$ , respectively.

### 3.4. $\text{BaCu}_{1.14}\text{In}_{0.86}\text{P}_2$ simulations

The unit cell of  $\text{BaCu}_{1.14}\text{In}_{0.86}\text{P}_2$  contains 10 atoms and its space group type is  $I4/mmm$  (number 139). The experimental lattice parameters at 175 K are  $a = b = 4.0073 \text{ \AA}$  and  $c = 13.451 \text{ \AA}$ , which were used for MD calculations. Cu and In share a  $4d$  site and P occupies a  $4e$  site. Ba mainly resides at the  $2a$  site, but the Ba site is reported as triple-split; 82% of Ba is at the  $2a$  site, while 18% of Ba are at a  $4e$  site very close to the  $2a$  site (at  $z = \pm 0.02$  compared to  $z = 0$  at the  $2a$  site).

$6 \times 6 \times 2$  supercells were used for MD simulations, which contain 144, 164, 124, and 288 Ba, Cu, In, and P atoms, respectively, or  $72(\text{BaCu}_{1.139}\text{In}_{0.861}\text{P}_2)$ . 10 supercells were

prepared as initial structures. The Cu and In atoms were randomly assigned to the 288 Cu/In sites. All Ba were initially positioned at the center of the triple split sites, namely the  $2a$  site, assuming that Ba can move to the  $4e$  site, as necessary, during the initial equilibration steps. The time step was 2 fs, positions were recorded every 100 steps, and 55,000 steps (110 ps, 500 position recordings) were considered. The first 5,000 steps (10 ps, 50 position recordings) were discarded as equilibration steps. The temperature  $T$  was varied between 25 to 300 K in 25 K intervals.

The final  $\mathbf{U}$  was obtained similarly as in  $\text{Ag}_8\text{SnSe}_6$ . The  $I4/mmm$  symmetry forces  $U^{11}=U^{22}$  and  $U^{23}=U^{13}=U^{12}=0$ , although this is not exactly attained with statistical handling of atom positions. The quantities  $(U^{11}+U^{22})/2$  (simply denoted as  $U^{11}$  for brevity),  $U^{33}$ , and the isotropic  $U_{\text{iso}}=(U^{11}+U^{22}+U^{33})/3$  were evaluated in this study.

#### 4. Results and discussion

The computational ADPs are those of individual atoms (ADP by atom) unless noted otherwise, while the experimental ADPs are as-reported values of ADP by site.

##### 4.1. $\text{Ag}_8\text{InSe}_6$

Figs. 2(a,b) show the ADPs for Ag obtained from  $2\times 2\times 2$  and  $3\times 3\times 3$  supercells, respectively. The isotropic ADP ( $U_{\text{iso}}$ ) is given for Ag2, Ag3, and Ag5 while the three eigenvalues of the ADP are provided, as  $U_1 < U_2 < U_3$ , to be consistent with Fig. 3. in Takahashi et al. (Takahashi *et al.*, 2024), which is reproduced as Fig. 2(c) with the same symbols and scales as in Figs. 2(a,b). The  $2\times 2\times 2$  and  $3\times 3\times 3$  supercell results are very similar, suggesting good convergence, and have roughly the same values as the experimental results in Fig. 2(c). However, there are minor differences. Ag3  $U_1$  and  $U_2$  approaches 0 as temperature  $T \rightarrow 0$  in calculations, but this is not the case in experiment.

The principal semi-axis lengths of the ellipsoid, which are the three eigenvalues of the matrix  $\mathbf{U}$ , help understand the shape of the ellipsoid. The calculated  $U$  values are  $U_1 < U_2 \ll U_3$  and  $U_1 \ll U_2 < U_3$  in Ag1 and Ag3 respectively, resulting in a cigar-like (prolate) and saucer-like (oblate) ellipsoid, respectively, as expected from experimental results. The calculated Ag1  $U_1$ , Ag1  $U_2$ , Ag3  $U_2$ , and Ag5  $U_{\text{iso}}$  are proportional to temperature over the entire shown temperature range, as is indicated in the linear fit that pass through the origin in Figs. 2(a,b). Other calculated  $\mathbf{U}$  values appear to approach  $\mathbf{U} \rightarrow 0$  in the limit  $T \rightarrow 0$  with the clear exception of Ag3  $U_3$ . The Ag3  $U_3$  value for 50 K is surprisingly larger than the 100 K value in the  $2\times 2\times 2$  supercell.



The Ag1 and Ag3 sites are almost three-fold trigonal planar coordinated. The experimental Ag-Se distances for Ag1 are 2.653, 2.659, and 2.707 Å, while those for Ag3 are 2.541, 2.687, and 2.774 Å, respectively. The chemical pressure from the very short Ag3-Se distance of 2.541 Å strongly motivates Ag to rattle in the direction out of the coordination plane (Takahashi *et al.*, 2024), which can effectively result in a split site. This rattling mechanism caused by from “retreat from stress” is found in tetrahedrites and tennantites  $(\text{Cu,Zn})_{12}(\text{Sb,As})_4\text{S}_{13}$ . (Suekuni *et al.*, 2018) The chemical pressure is much weaker for Ag1, thus Ag1 can be a non-split site while a similarly coordinated Ag3 may be a split site in the direction almost normal to the three-fold coordination plane. Experimentally, all of  $U_1$ ,  $U_2$ , and  $U_3$  of Ag3 do not approach  $U \rightarrow 0$  in the limit  $T \rightarrow 0$ , which is also a hint of site splitting.

Fig. 3 is a schematic of a double-split site for qualitative discussion on the temperature ( $T$ ) dependence of  $U$  by atom. The energy is proportional to  $T$ . At very low  $T$  ( $T_1$ ), the atom is trapped in one of the wells, resulting in a small  $U$ .  $T$  that allows atoms to move between the wells, for example by thermal fluctuation or tunneling, but is sufficiently low that atoms still reside in one of the wells ( $T_2$ ) result in a very large  $U$  because the atom is typically located far from the average position between the wells. Further increasing  $T$  such that the atom is effectively in a single well ( $T_3$ ) results in substantial decrease in  $U$  because the atom can now be at the center of the well. Gradually increasing  $T$  ( $T_4$ ) results in a gradually increasing  $U$ . The  $U$  by atom and  $U$  by site should be almost the same for  $T \geq T_2$ , but, at  $T_1$ , the  $U$  by site is expected to be much larger than  $U$  by atom because atoms can occupy both wells of the site.

Tables 2 and 3 show the elements of  $\mathbf{U}$ , the eigenvalues  $U_1$ ,  $U_2$ , and  $U_3$ ,  $U_3/U_1$ , and  $U_{\text{iso}}$  for all Ag sites at 200 K and 300 K, respectively, from the  $3 \times 3 \times 3$  supercell simulations. Ref. (Takahashi *et al.*, 2024) used anisotropic  $\mathbf{U}$  for Ag1 and Ag3 because this dramatically improved the  $R_{\text{wp}}$  of experimental data at 300 K. Calculations can provide anisotropic  $\mathbf{U}$  for all Ag simultaneously and independently without the need for repeated refinement attempts. The calculated value of a measure of anisotropy,  $U_3/U_1$ , at 300K is roughly 3.5 for Ag1, Ag3, and Ag5 (Table 3). The  $U_{\text{iso}}$  of Ag3 is roughly double of Ag1 and Ag5, and the number of Ag5 atoms is half of Ag1. Therefore, considering anisotropy of Ag5 might result in a smaller improvement of  $R_{\text{wp}}$  compared to Ag1 and Ag 3. Ag2 and Ag4 are less anisotropic than Ag1, Ag3, and Ag5 because of their smaller  $U_3/U_1$ , thus using anisotropic  $\mathbf{U}$  would not improve  $R_{\text{wp}}$  significantly. The trends are similar for both

200 K (Table 2) and 300 K (Table 3).

#### 4.2. Na<sub>2</sub>In<sub>2</sub>Sn<sub>4</sub>

Fig. 4 shows the eigenvalues of experimental (Yamada *et al.*, 2023) and calculated  $U$ , denoted as  $U_1 < U_2 < U_3$ , for Na and In/Sn1 sites. ( $U_a$  is used instead of  $U_3$  in the original reference.) The results for In/Sn2 and In/Sn3 sites are very similar to the In/Sn1 sites and are not shown. The In and Sn  $U$  are calculated separately, although one  $U$  for In and Sn combined is obtained experimentally.

The experimental and computational  $U$  values of Na are comparable to each other, and  $U_3$  of Na is significantly larger than  $U_1$  and  $U_2$  for all temperatures, implying an almost cigar-shaped spheroid. (Fig. 4(a)) The experimental  $U_1$ ,  $U_2$ , and  $U_3$  are roughly proportional to  $T$  (linear regressions passing through the origin are shown in black lines). The calculated  $U$  is roughly the same as the experimental  $U$ , but the details are slightly different. All of  $U_1$ ,  $U_2$ , and  $U_3$  are almost proportional to  $T$  up to about 150 K, but consistently becomes larger than the linear regression of 50, 100, and 150 K values that passes through the origin (shown as red solid lines below 175 K, extrapolations to higher temperature shown with dashed lines above 175 K).

This deviation from proportionality in calculations is even more profound in In/Sn1 sites. The calculated  $U_3$  of In1 is comparable to the  $U_3$  of Na at 300 K, which is very different from the experimental results! (Fig. 4(b)) However, the experimental and computational  $U$  values are relatively close to each other at 50 and 100 K (Fig. 4(c), which is an enlargement of Fig. 4(b) at low  $U$ ).

A large  $U$  value results in a large displacement from the equilibrium position. The standard deviation of the atom position,  $\sigma$ , is simply the square root of  $U$ . A  $U$  of  $0.09 \text{ \AA}^2$  along a certain direction corresponds to a  $\sigma$  of  $0.3 \text{ \AA}$ . Assuming a normal distribution, the atom is more than  $3\sigma = 0.9 \text{ \AA}$  away from the average position for 0.3% of the time. This  $0.9 \text{ \AA}$  is roughly one-third of the In/Sn-In/Sn bond length ( $\sim 2.87 \text{ \AA}$ ).

In the author's previous study on LaH<sub>2.75</sub>O<sub>0.125</sub>, (Hinuma, 2025) the isotropic ADP of O,  $U_{\text{iso}}$  (denoted as  $\langle \Delta r^2 \rangle$  in the reference), is roughly proportional to temperature below  $\sim 0.02 \text{ \AA}^2$  but becomes much larger than what is expected from the proportionality trend above this threshold  $U_{\text{iso}}$  value. The  $U_{\text{iso}}$  of La is proportional up to  $\sim 0.03 \text{ \AA}^2$ , which covers the entire considered range of  $T$ . This LaH<sub>2.75</sub>O<sub>0.125</sub> is known as a very good H ion

conductor. The H and O, together with vacancies, share the same sublattice in  $\text{LaH}_{2.75}\text{O}_{0.125}$ , thus O may easily move away from the original site after a very small displacement on the order of  $\sim 0.1 \text{ \AA}$  from the equilibrium position.

Inspection of atom movements during MD simulations of  $\text{Na}_2\text{In}_2\text{Sn}_4$  revealed significant displacements of atoms at  $T \geq 200 \text{ K}$ . The increase in  $U$  above the proportionality trend in calculations, but not in experiment, is caused by the difference in how  $U$  is obtained. Experimentally, the displacement of atoms is the distance to the nearest atom site, and the same diffusing atom may be assigned to different sites as time progresses. In contrast, the displacement in calculations is always the distance to the original atom site. The calculated  $U$  overestimates the actual  $U$  when atoms can move away from the original site.

For the record, Table 4 shows calculated  $U$  values of Na together with reported experimental values at 200, 250, and 300 K. (Yamada *et al.*, 2023) The calculated and experimental values for 200, 250, and 300 K are consistent with each other, although the sign is different in some off-diagonal  $U$  coefficients.

### 4.3. $\text{BaCu}_{1.14}\text{Cu}_{0.86}\text{P}_2$

Table 5 shows the calculated  $U$  of  $\text{BaCu}_{1.14}\text{In}_{0.86}\text{P}_2$  at 175 K together with experimental results (Sarkar *et al.*, 2024) at 173 K. In the reference, the same  $U_{\text{iso}}$  was provided for each split Ba site, and anisotropic  $U$  was not given for Ba. Anisotropic  $U$  was provided for the Cu/In and P sites. Experimentally, the Cu/In site has the largest  $U$  and is moderately anisotropic with  $U^{33}/U^{11}=1.38$ , while the  $U$  of P is very anisotropic with  $U^{33}/U^{11}=2.24$  and is slightly smaller than that of Cu/In. The calculations underestimate experimentally determined  $U$ . Notably, the calculated  $U^{33}$  of Cu/In and P are roughly one-half and one-third of the experimental  $U^{33}$ , respectively.

Fig. 5 shows the calculated anisotropic  $U$  of Ba and Cu and isotropic  $U_{\text{iso}}$  of In and P. The  $U_{\text{iso}}$  of In and P are almost the same value for all temperatures  $T$ . All atoms are in an almost harmonic potential, with the linear regressions passing very close to the origin although not required to do so. There were no migrating atoms.

The difference in  $U$  between experiment and calculations in Table 5 arises from how the values were derived. The experimental ADPs are by site, while the calculated ADPs in Table 5 and Fig. 5 are the averages of ADPs by atom. Therefore, the  $U^{33}$  by site was

additionally derived using a histogram of  $z$ -coordinates. Atoms with coordinates outside of  $-0.1 < z < 0.4$  were translated, in integer multiples of 0.5, to this range; note that  $\text{BaCu}_{1.14}\text{In}_{0.86}\text{P}_2$  is a body-centered crystal.

Figs. 6(a-d) show the histograms for Ba, Cu, In, and P, respectively, for  $T = 50, 175,$  and  $300$  K. The bin size of the  $z$ -coordinate is 0.001. There are  $144 \text{ atoms} \times 500 \text{ position recordings} \times 10 \text{ supercells} = 720,000$  total positions for Ba. Only the  $z \approx 0.14$  peak is shown for P (there is another peak at  $z \approx -0.14$ , which is a mirror image around  $z = 0$ , that is not shown). The normal distribution regressions and their standard deviations are also given, which can be used to obtain the ADP by site. The histogram for Cu in Fig. 6(b) cannot be described well by a single normal distribution.

The curve for Ba is single peak, and the experimentally suggested triple well scenario with small peaks at  $\Delta z = \pm 0.02$  (Sarkar *et al.*, 2024) is clearly denied. In contrast, Cu, but not In, shows a triple peak with additional peaks at  $\Delta z \approx \pm 0.025$ . Figs. 6(e) and (f) shows the histograms of Cu and Cu/In combined, respectively, for  $T = 50$  and  $175$  K and the regressions

$$y = A \left[ p \exp \left\{ -\frac{(z-0.25)^2}{2\sigma^2} \right\} + \frac{1-p}{2} \exp \left\{ -\frac{(z-0.25-\Delta z)^2}{2\sigma^2} \right\} + \frac{1-p}{2} \exp \left\{ -\frac{(z-0.25+\Delta z)^2}{2\sigma^2} \right\} \right]. \quad (15)$$

The values to be fitted are a scaling constant  $A$ , the occupancy ratio of the main peak  $p$ , the standard deviation of the peaks  $\sigma$ , and the position of the additional peaks  $\Delta z$ . Equation 15 provides a very good fit, and the parameters used in fitting are given in Table 6. Very interestingly, the  $p$  for Cu/In at  $175$  K is 0.811, which is the experimental occupancy of the main peak of Ba. The  $\Delta z$  of Ba in the experiment is 0.021, while the  $\Delta z$  of Cu/In in the calculation is a very similar value of 0.026.

Fig. 7 plots the calculated  $U^{33}$  ADP by atom and by site. The site ADP is obtained as

$$U_{\text{site}}^{33} = c^2 \sigma^2 \quad \text{where } c \text{ is the lattice parameter and } \sigma \text{ is the standard deviation of the}$$

histogram. The ADP was obtained for Cu only, In only, and Cu/In combined for the  $4d$  site. A single normal distribution and a superimposition of three normal distributions with same  $\sigma$  as in equation 15, which models a triple-split site, were calculated with Cu and Cu/In sites.

In Fig. 7, all shown  $U^{33}$  are well described with linear fits. The extrapolation of  $U^{33}$  when  $T \rightarrow 0$  is non-zero for all  $U^{33}$  by site. There is no thermal fluctuation at  $T \rightarrow 0$ , thus describing the non-zero ADPs at  $T \rightarrow 0$  as “temperature factors”, “thermal ellipsoids”, thermal displacement parameters” and the like is nothing other than inappropriate. The non-zero ADPs are the result of disorder of Cu/In sites that cause atoms to move away from the average atom sites defined as points.

The calculated  $U^{33}$  by site at 175 K for Cu/In with split sites and P, which are 0.0186 and 0.0215  $\text{\AA}^2$ , respectively, are very close to the experimental results at 173 K of 0.0222 and 0.0208  $\text{\AA}^2$ , respectively. The difference between experimental and calculated results in Table 5 therefore originate from the averaging process used to obtain the ADP.

## 5. Summary

The anisotropic ADPs by atom were directly derived from MD simulations taking the (co)variances over atom positions at different time steps. The ADPs can be obtained by atom, where the (co)variance of each atom is obtained and then averaged for atoms in an atom site, or by site, where the (co)variance is calculated over all atoms at the atom site. The experimentally obtained shapes of anisotropic displacement ellipsoids of rattling atoms in thermoelectric materials  $\text{Ag}_8\text{SnSe}_6$  and  $\text{Na}_2\text{In}_2\text{Sn}_4$  are consistent with calculated results. The possibility of splitting of the Ag3 site of  $\text{Ag}_8\text{SnSe}_6$  can be detected through calculation of the ADP over different temperatures. Migration of atoms was found in  $\text{Na}_2\text{In}_2\text{Sn}_4$  at  $T \geq 200$  K, resulting in a very large ADP by atom that disagrees with the experimentally obtained, much smaller ADPs by atom site. The ADPs by atom and by site is clearly different in the thermoelectric material  $\text{BaCu}_{1.14}\text{In}_{0.86}\text{P}_2$ , which is caused by disorder in the shared Cu/In site. The non-zero ADPs by site at  $T \rightarrow 0$  in  $\text{BaCu}_{1.14}\text{In}_{0.86}\text{P}_2$  is a good reason why ADPs should not be referred to as “temperature factors” or “thermal ellipsoids” because the non-zero ADPs are the result of disorder of Cu/In atoms. The investigations in this study suggest the effectiveness and limitations of direct ADP derivation from MD simulations and the use of calculated ADPs as a tool complementing experimental efforts to determine the crystal structure including atom displacement around atom sites.

## Acknowledgments

The author thanks Dr. Nishibori for sharing data used to draw Fig. 3 in Ref (Yamada *et al.*, 2023), which was used to draw Fig. 2(c) in this paper. This study was funded by a Kakenhi Grant-in-Aid (No. 24H00395) from the Japan Society for the Promotion of

Science (JSPS). The VESTA code (Momma & Izumi, 2011) was used to draw Figure 1.

## References

- Erba, A., Ferrabone, M., Orlando, R. & Dovesi, R. (2013). *J. Comput. Chem.* **34**, 346-354.
- Grosse-Kunstleve, R. W. & Adams, P. D. (2002). *J. Appl. Crystallogr.* **35**, 477-480.
- Hinuma, Y. (2025). *Comp. Mater. Sci.* **246**, 113368.
- Hoover, W. G. (1985). *Phys. Rev. A* **31**, 1695-1697.
- Kresse, G. & Furthmüller, J. (1996). *Phys. Rev. B* **54**, 11169-11186.
- Kresse, G. & Joubert, D. (1999). *Phys. Rev. B* **59**, 1758-1775.
- Lane, N. J., Vogel, S. C., Hug, G., Togo, A., Chaput, L., Hultman, L. & Barsoum, M. W. (2012). *Phys. Rev. B* **86**, 214301.
- Madsen, A. O., Civalleri, B., Ferrabone, M., Pascale, F. & Erba, A. (2013). *Acta Crystallographica Section A* **69**, 309-321.
- Momma, K. & Izumi, F. (2011). *J. Appl. Crystallogr.* **44**, 1272-1276.
- Nosé, S. (1984). *J. Chem. Phys.* **81**, 511-519.
- Perdew, J. P., Burke, K. & Ernzerhof, M. (1996). *Phys. Rev. Lett.* **77**, 3865-3868.
- Reilly, A. M., Wann, D. A., Gutmann, M. J., Jura, M., Morrison, C. A. & Rankin, D. W. H. (2013). *J. Appl. Crystallogr.* **46**, 656-662.
- Reilly, A. M., Wann, D. A., Morrison, C. A. & Rankin, D. W. H. (2007). *Chem. Phys. Lett.* **448**, 61-64.
- Sarkar, A., Porter, A. P., Viswanathan, G., Yox, P., Earnest, R. A., Wang, J., Rossini, A. J. & Kovnir, K. (2024). *Journal of Materials Chemistry A* **12**, 10481-10493.
- Suekuni, K., Lee, C. H., Tanaka, H. I., Nishibori, E., Nakamura, A., Kasai, H., Mori, H., Usui, H., Ochi, M., Hasegawa, T., Nakamura, M., Ohira-Kawamura, S., Kikuchi, T., Kaneko, K., Nishiate, H., Hashikuni, K., Kosaka, Y., Kuroki, K. & Takabatake, T. (2018). *Adv. Mater.* **30**, 1706230.
- Takahashi, S., Kasai, H., Liu, C., Miao, L. & Nishibori, E. (2024). *Crystal Growth & Design* **24**, 6267-6274.
- Takamoto, S., Shinagawa, C., Motoki, D., Nakago, K., Li, W., Kurata, I., Watanabe, T., Yayama, Y., Iriguchi, H., Asano, Y., Onodera, T., Ishii, T., Kudo, T., Ono, H., Sawada, R., Ishitani, R., Ong, M., Yamaguchi, T., Kataoka, T., Hayashi, A., Charoenphakdee, N. & Ibuka, T. (2022). *Nat. Commun.* **13**, 2991.
- Trueblood, K. N., Burgi, H.-B., Burzlaff, H., Dunitz, J. D., Gramaccioni, C. M., Schulz, H. H., Shmueli, U. & Abrahams, S. C. (1996). *Acta Crystallographica Section A* **52**, 770-781.
- Yamada, T., Yoshiya, M., Kanno, M., Takatsu, H., Ikeda, T., Nagai, H., Yamane, H. & Kageyama, H. (2023). *Adv. Mater.* **35**, 2207646.

**Table 1.** Notations of position and displacement vectors, bases, and ADPs.

| Basis                  | Direct lattice ( <b>a</b> , <b>b</b> , <b>c</b> ) or ( <b>a</b> <sub>1</sub> , <b>a</b> <sub>2</sub> , <b>a</b> <sub>3</sub> ) | Direct lattice ( <i>a</i> <sup>*</sup> <b>a</b> , <i>b</i> <sup>*</sup> <b>b</b> , <i>c</i> <sup>*</sup> <b>c</b> ) or ( <i>a</i> <sup>1</sup> <b>a</b> <sub>1</sub> , <i>a</i> <sup>2</sup> <b>a</b> <sub>2</sub> , <i>a</i> <sup>3</sup> <b>a</b> <sub>3</sub> ) | Cartesian basis ( <b>e</b> <sub>1</sub> , <b>e</b> <sub>2</sub> , <b>e</b> <sub>3</sub> )                     |
|------------------------|--|--|---|
| Components of <b>r</b> | <i>x</i> , <i>y</i> , <i>z</i> or <i>x</i> <sup>1</sup> , <i>x</i> <sup>2</sup> , <i>x</i> <sup>3</sup>                        | $\xi$ , $\eta$ , $\zeta$ or $\xi^1$ , $\xi^2$ , $\xi^3$  | $\xi^C$ , $\eta^C$ , $\zeta^C$ or $\xi^C_1$ , $\xi^C_2$ , $\xi^C_3$   |
| Components of <b>u</b> | $\Delta x$ , $\Delta y$ , $\Delta z$ or $\Delta x^1$ , $\Delta x^2$ , $\Delta x^3$   | $\Delta \xi$ , $\Delta \eta$ , $\Delta \zeta$ or $\Delta \xi^1$ , $\Delta \xi^2$ , $\Delta \xi^3$  | $\Delta \xi^C$ , $\Delta \eta^C$ , $\Delta \zeta^C$ or $\Delta \xi^C_1$ , $\Delta \xi^C_2$ , $\Delta \xi^C_3$ |
| Related ADP            | $\beta^{ij}=2\pi^2\langle\Delta x^i\Delta x^j\rangle$  | $U^{ij}=\langle\Delta \xi^i\Delta \xi^j\rangle$  | $U^C_{ij}=\langle\Delta \xi^C_i\Delta \xi^C_j\rangle$   |
| Unit of related ADP    | Dimensionless  | Length <sup>2</sup>  | Length <sup>2</sup>   |

**Table 2.** *U* of Ag in Ag<sub>8</sub>SnSe<sub>6</sub> at 200 K from 3×3×3 supercell MD simulations. The unit is Å<sup>2</sup>.

|     | <i>U</i> <sup>11</sup> | <i>U</i> <sup>22</sup> | <i>U</i> <sup>33</sup> | <i>U</i> <sup>23</sup> | <i>U</i> <sup>13</sup> | <i>U</i> <sup>12</sup> | <i>U</i> <sub>3</sub> | <i>U</i> <sub>2</sub> | <i>U</i> <sub>1</sub> | <i>U</i> <sub>3</sub> / <i>U</i> <sub>1</sub> | <i>U</i> <sub>iso</sub> |
|-----|------------------------|------------------------|------------------------|------------------------|------------------------|------------------------|-----------------------|-----------------------|-----------------------|---|-------------------------|
| Ag1 | 0.023                  | 0.023                  | 0.029                  | 0.007                  | 0.005                  | 0.010                  | 0.040                 | 0.022                 | 0.013                 | 3.1   | 0.025                   |
| Ag2 | 0.024                  | 0.028                  | 0.037                  | -0.004                 | 0.006                  | -0.001                 | 0.041                 | 0.026                 | 0.022                 | 1.9   | 0.030                   |
| Ag3 | 0.041                  | 0.066                  | 0.047                  | 0.005                  | -0.026                 | 0.009                  | 0.072                 | 0.066                 | 0.016                 | 4.4   | 0.051                   |
| Ag4 | 0.031                  | 0.029                  | 0.019                  | -0.004                 | 0.000                  | 0.000                  | 0.031                 | 0.030                 | 0.018                 | 1.7   | 0.026                   |
| Ag5 | 0.037                  | 0.023                  | 0.013                  | 0.004                  | 0.000                  | 0.000                  | 0.037                 | 0.025                 | 0.012                 | 3.2   | 0.024                   |

**Table 3.** *U* values of Ag in Ag<sub>8</sub>SnSe<sub>6</sub> at 300 K from 3×3×3 supercell MD simulations. The unit is Å<sup>2</sup>.

|     | <i>U</i> <sup>11</sup> | <i>U</i> <sup>22</sup> | <i>U</i> <sup>33</sup> | <i>U</i> <sup>23</sup> | <i>U</i> <sup>13</sup> | <i>U</i> <sup>12</sup> | <i>U</i> <sub>3</sub> | <i>U</i> <sub>2</sub> | <i>U</i> <sub>1</sub> | <i>U</i> <sub>3</sub> / <i>U</i> <sub>1</sub> | <i>U</i> <sub>iso</sub> |
|-----|------------------------|------------------------|------------------------|------------------------|------------------------|------------------------|-----------------------|-----------------------|-----------------------|---|-------------------------|
| Ag1 | 0.043                  | 0.040                  | 0.053                  | 0.015                  | 0.014                  | 0.020                  | 0.078                 | 0.036                 | 0.022                 | 3.6   | 0.045                   |
| Ag2 | 0.047                  | 0.054                  | 0.070                  | -0.017                 | -0.002                 | 0.005                  | 0.081                 | 0.049                 | 0.042                 | 2.0   | 0.057                   |
| Ag3 | 0.077                  | 0.114                  | 0.067                  | 0.011                  | -0.032                 | 0.015                  | 0.119                 | 0.103                 | 0.035                 | 3.4   | 0.086                   |
| Ag4 | 0.051                  | 0.073                  | 0.034                  | -0.009                 | 0.001                  | 0.001                  | 0.075                 | 0.051                 | 0.032                 | 2.4   | 0.053                   |
| Ag5 | 0.062                  | 0.038                  | 0.021                  | 0.007                  | -0.001                 | 0.000                  | 0.062                 | 0.041                 | 0.018                 | 3.4   | 0.041                   |

**Table 4.**  $U$  of Na in  $\text{Na}_2\text{In}_2\text{Sn}_4$  derived from MD simulations at various temperatures  $T$ . Experimental values from Yamada et al. (Yamada *et al.*, 2023) are shown in brackets. Units of  $T$  and  $U$  are K and  $\text{\AA}^2$ , respectively.

| $T$ | $U^{11}$ | $U^{22}$ | $U^{33}$ | $U^{23}$ | $U^{13}$ | $U^{12}$ |
|-----|----------|----------|----------|----------|----------|----------|
| 50  | 0.009    | 0.009    | 0.009    | -0.004   | -0.005   | 0.005    |
| 100 | 0.020    | 0.021    | 0.018    | -0.009   | -0.011   | 0.011    |
| 150 | 0.033    | 0.033    | 0.028    | -0.015   | -0.017   | 0.019    |
| 200 | 0.046    | 0.047    | 0.039    | -0.021   | -0.024   | 0.030    |
|     | (0.055)  | (0.051)  | (0.048)  | (-0.024) | (-0.033) | (0.036)  |
| 250 | 0.072    | 0.070    | 0.065    | -0.029   | -0.036   | 0.037    |
|     | (0.072)  | (0.065)  | (0.061)  | (0.049)  | (-0.043) | (-0.032) |
| 300 | 0.092    | 0.088    | 0.094    | -0.029   | -0.051   | 0.034    |
|     | (0.087)  | (0.078)  | (0.073)  | (-0.040) | (0.055)  | (0.060)  |

**Table 5.**  $U$  of  $\text{BaCu}_{1.14}\text{In}_{0.86}\text{P}_2$  at 175 K (Sarkar *et al.*, 2024). Values from MD simulations are shown together with experimental values from Sarkar et al. (Sarkar *et al.*, 2024) In Sarkar et al. (Sarkar *et al.*, 2024), the  $U_{\text{iso}}$  of Ba is the same for Ba1 and Ba11 sites and the ADP of Ba is not given, and only the combined ADP is provided for Cu/In sites. The Cu/In values from calculations, shown in brackets, are the 164:124 weighted averages based on the Cu/In atom ratio. The unit of  $U$  is  $\text{\AA}^2$ .

| $T$   | Calculated |          |                 |                  | Experiment |          |                 |                  |
|-------|------------|----------|-----------------|------------------|------------|----------|-----------------|------------------|
|       | $U^{11}$   | $U^{33}$ | $U^{33}/U^{11}$ | $U_{\text{iso}}$ | $U^{11}$   | $U^{33}$ | $U^{33}/U^{11}$ | $U_{\text{iso}}$ |
| Ba    | 0.0077     | 0.0100   | 1.31            | 0.0085           |            |          |                 | 0.0103           |
| Cu    | 0.0113     | 0.021    | 1.68            | 0.0139           |            |          |                 |                  |
| In    | 0.0066     | 0.070    | 1.08            | 0.0068           |            |          |                 |                  |
| Cu/In | (0.0093)   | (0.0139) | (1.50)          | (0.0108)         | 0.0165     | 0.0222   | 1.38            | 0.0184           |
| P     | 0.0070     | 0.0070   | 1.01            | 0.0070           | 0.0093     | 0.0208   | 2.24            | 0.0131           |

**Table 6.** Parameters used to fit curves in Fig. 6(e,f) using equation 15.

| Elements | $T$ (K) | $A$ ( $10^3$ ) | $p$  | $\sigma$ | $\Delta z$ |
|----------|---------|----------------|------|----------|------------|
| Cu       | 175     | 28.4           | 0.66 | 0.0115   | 0.0257     |
| Cu       | 50      | 35.1           | 0.63 | 0.0092   | 0.0257     |
| Cu/In    | 175     | 56.3           | 0.81 | 0.0101   | 0.0264     |
| Cu/In    | 50      | 67.4           | 0.79 | 0.0084   | 0.0257     |



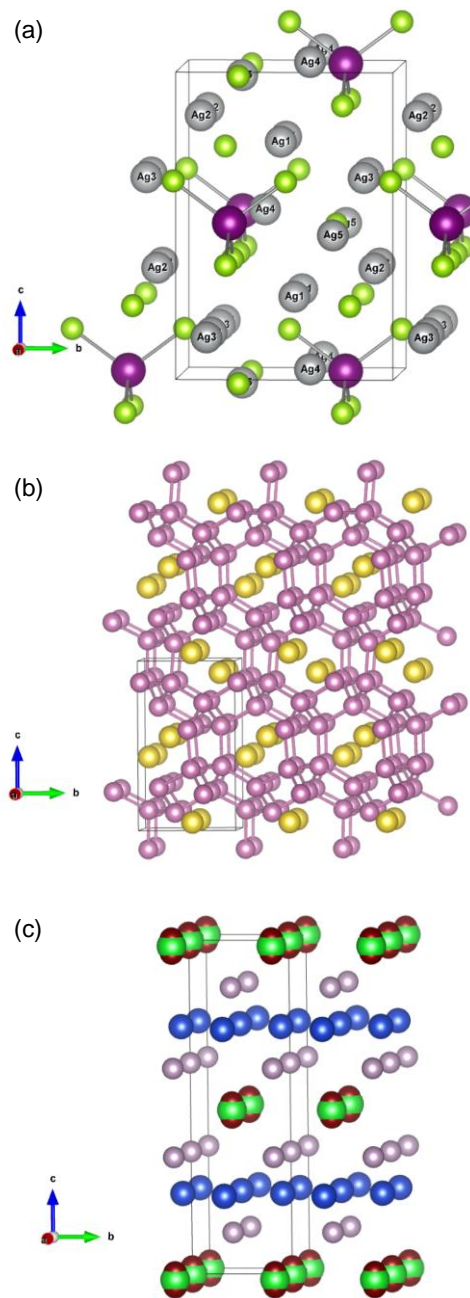


Fig. 1. Experimentally obtained crystal structures of (a)  $\text{Ag}_8\text{SnSe}_6$  (Takahashi *et al.*, 2024), (b)  $\text{Na}_2\text{In}_2\text{Sn}_4$  (Yamada *et al.*, 2023), and (c)  $\text{BaCu}_{1.14}\text{Cu}_{0.86}\text{P}_2$  (Sarkar *et al.*, 2024). (a) Gray, dark purple, and green circles represent Ag, Sn, and Se sites respectively. (b) Yellow and purple circles represent Na and In/Sn sites, respectively. (c) Green, blue, and light purple circles represent the main Ba, Cu/In, and P sites, respectively. The small brown circles above and below large green circles are the Ba11 sites in ref. (Sarkar *et al.*, 2024). This reference claims that the Ba site is triple-split where most of the Ba occupies the main Ba1 site (green circles) but about 18% enters Ba11 sites at 175 K.

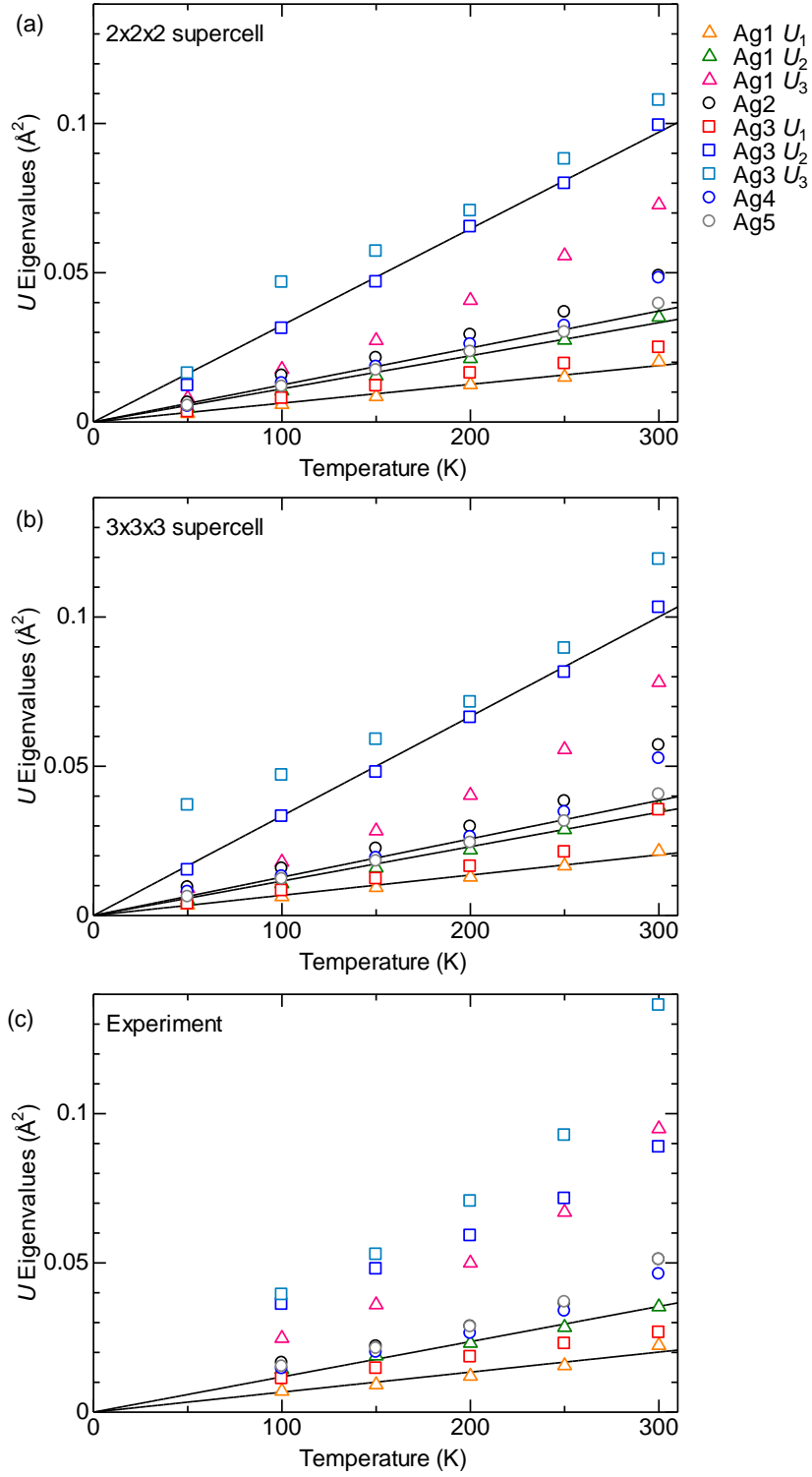


Fig. 2. (a,b) Computational and (c) experimental  $U$  values of  $\text{Ag}_8\text{InSe}_6$ . The displayed quantities and their symbols are the same as experimental data (shown in (c)) in Ref. (Yamada *et al.*, 2023). Linear regressions pass through the origin.

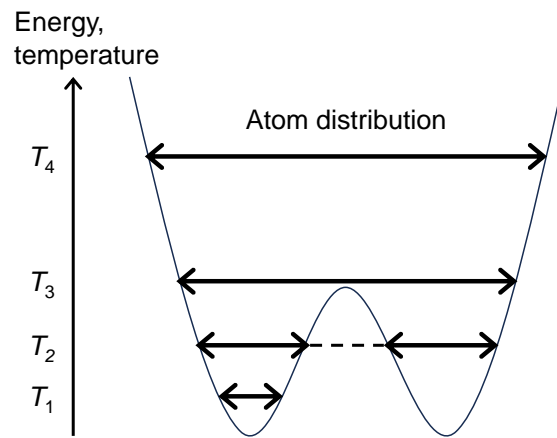


Fig. 3. Schematic of atom distribution in a double well potential.

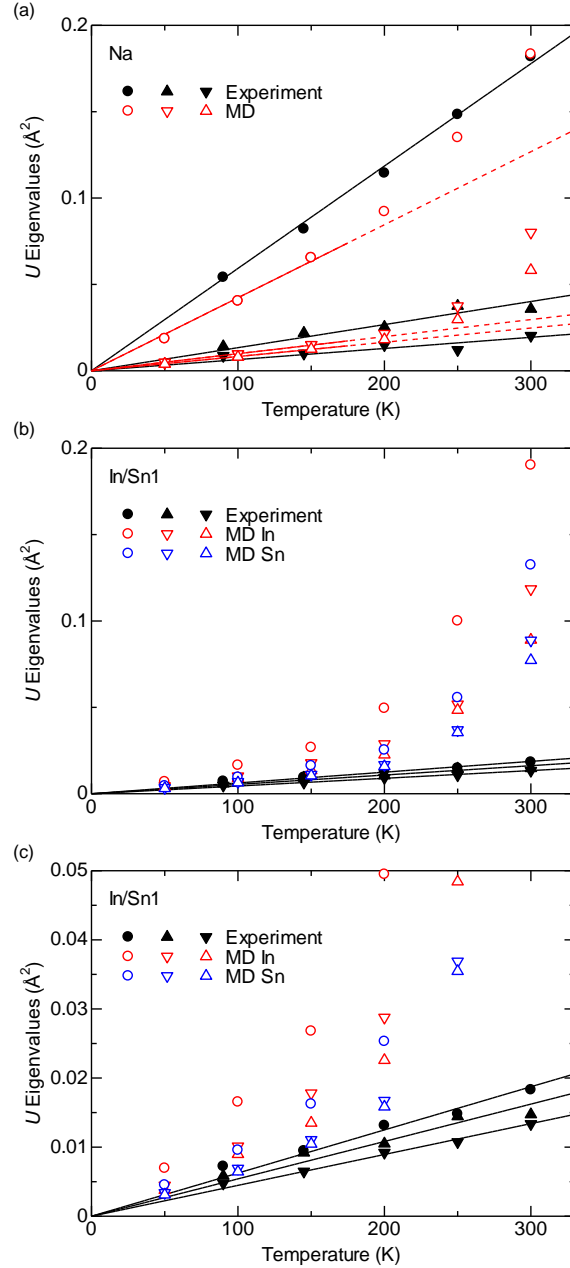


Fig. 4. The eigenvalues of experimental (Yamada *et al.*, 2023) and calculated  $U$  of  $\text{Na}_2\text{In}_2\text{Sn}_4$ , of (a) Na and (b.c) In/Sn sites, shown with different symbols, plotted against temperature. (c) is an enlargement of (b) for small  $U$ . Experimental values are shown with black filled symbols and the linear regressions passing through the origin are shown with solid lines. Computational values are shown with empty symbols and the linear regressions in (a) passing through the origin for 50, 100, and 150 K points are shown with solid lines at  $T < 175$  K and are extrapolated using dashed lines at  $T > 175$  K.

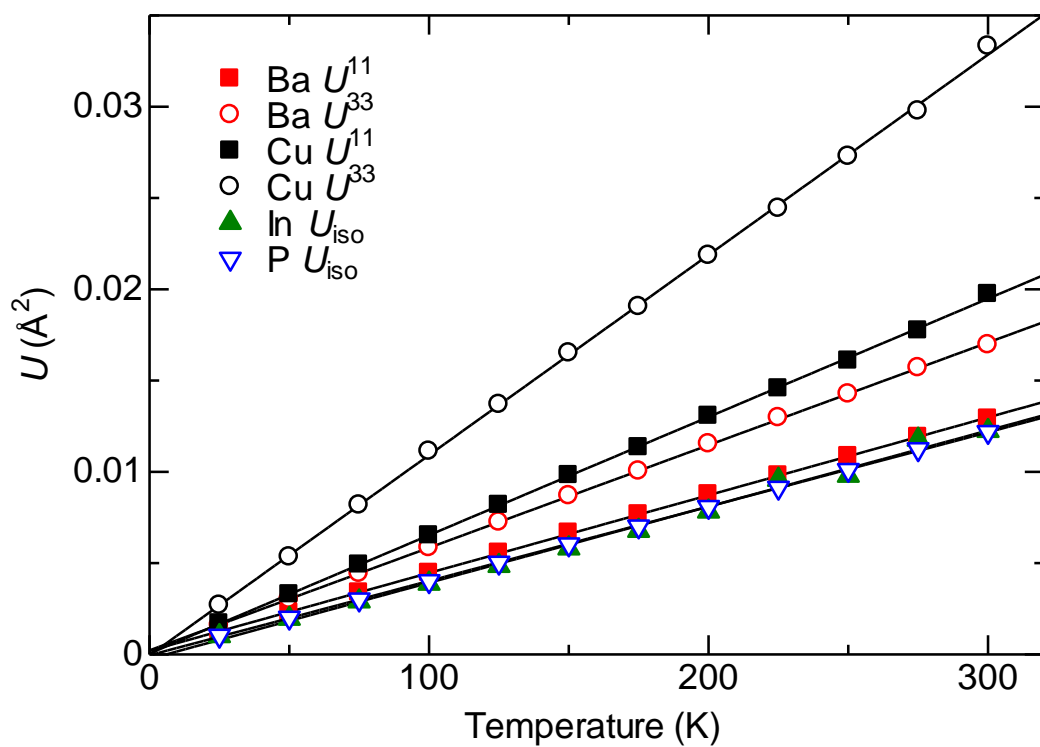


Fig. 5. Calculated  $U$  values by atom for  $\text{BaCu}_{1.14}\text{In}_{0.86}\text{P}_2$ . The anisotropic  $U^{11}$  and  $U^{33}$  are given for Ba and Cu because of their large anisotropy, and isotropic  $U_{iso}$  is plotted for In and P with low anisotropy. The linear regressions in solid lines are not forced to pass through the origin.

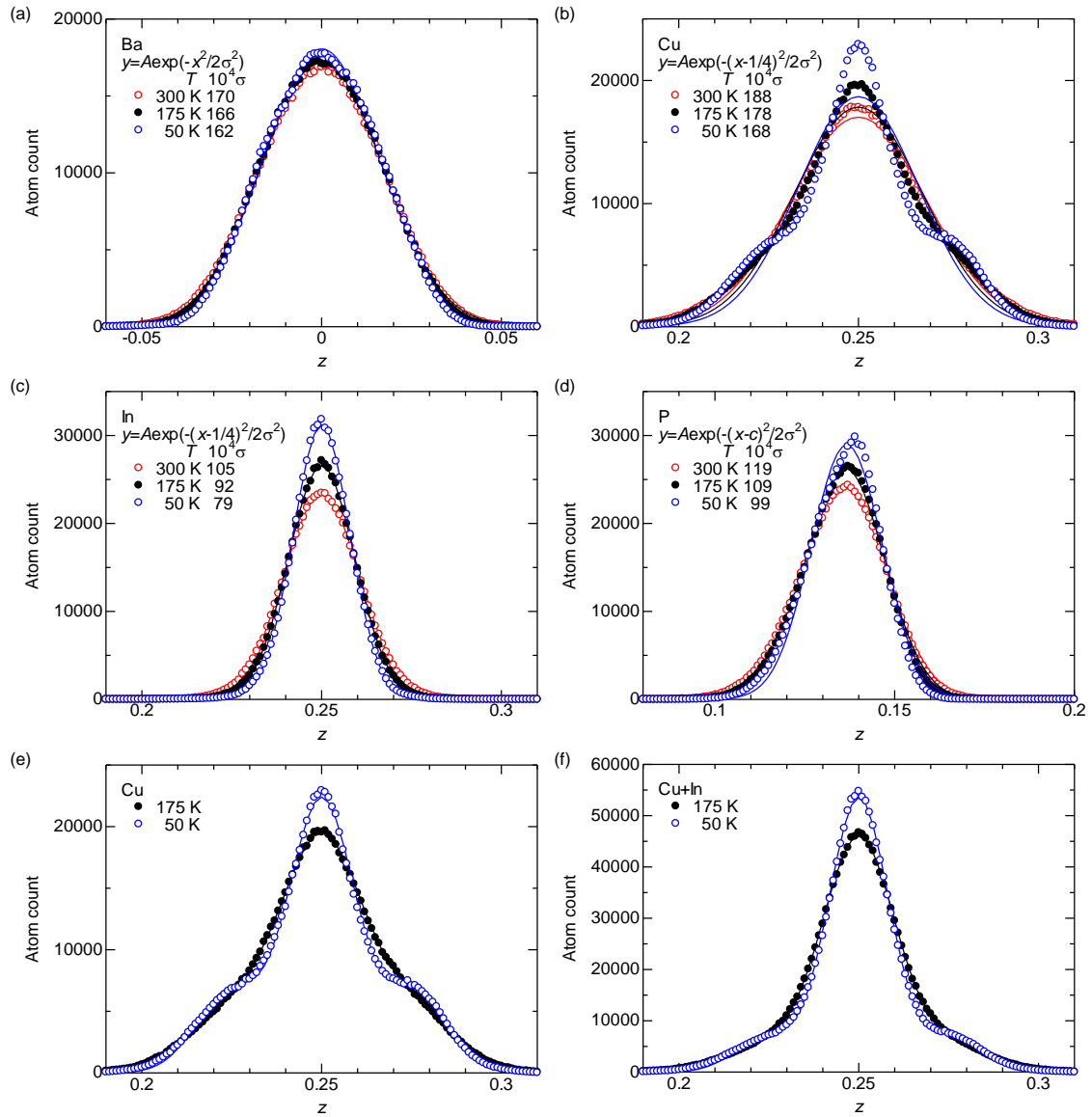


Fig. 6. Distribution of  $z$  coordinates of (a) Ba, (b,e) Cu, (c) In, (d) P, and (f) Cu+In combined in  $\text{BaCu}_{1.14}\text{In}_{0.86}\text{P}_2$  derived from the atom positions obtained from MD simulations. The atom positions were binned with 0.001 intervals of  $z$ . The points are fitted to (a-d) normal distributions (solid lines) and (e,f) superimposition of three normal distributions in equation 15. The standard deviation  $\sigma$  of the distributions are shown in (a-d).

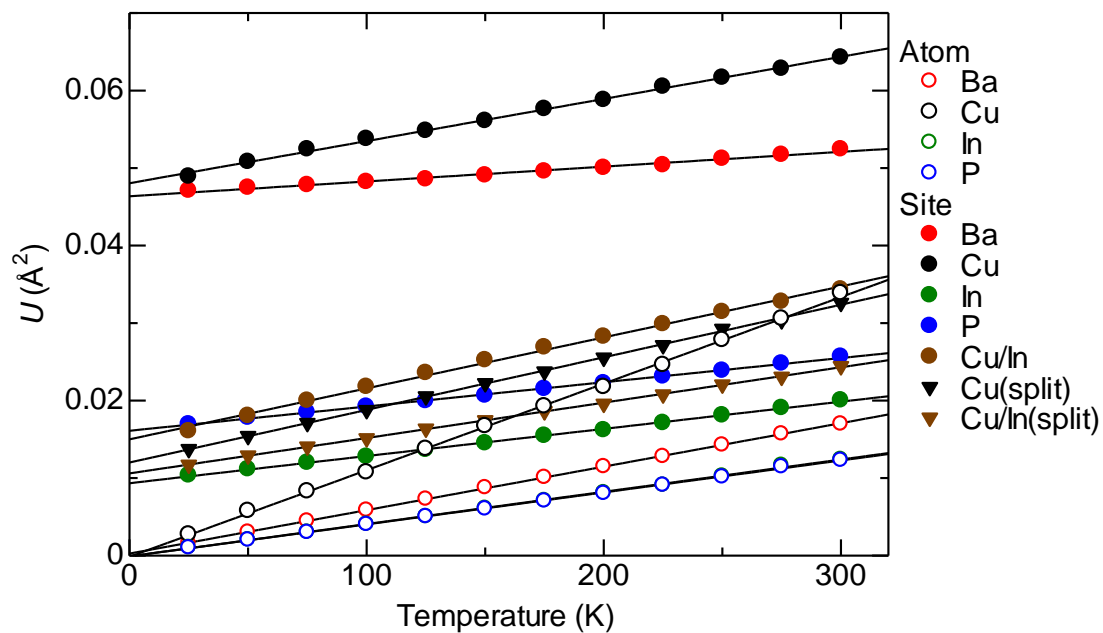


Fig. 7.  $U^{33}$  per atom (empty symbols) and by site (filled symbols). The  $U^{33}$  by site is the variance of the normal distribution fit as in Fig. 6. The variance from fitting of three superimposed normal distribution with same valences are shown for Cu and Cu/In sites (triangular symbols for “split” sites).